HHS Public Access

Author manuscript

Nat Struct Mol Biol. Author manuscript; available in PMC 2017 June 05.

Published in final edited form as:

Nat Struct Mol Biol. 2017 January ; 24(1): 30–39. doi:10.1038/nsmb.3335.

A balance between elongation and trimming regulates telomere stability in stem cells

Teresa Rivera[1], **Candy Haggblom**[1], **Sandro Cosconati**[2], and **Jan Karlseder**[1,*]

[1]Molecular and Cellular Biology Department, The Salk Institute for Biological Studies, 10010 North Torrey Pines Rd., La Jolla, CA 92037, USA

[2]DiSTABiF, Second University of Naples, Via Vivaldi 43, 81100 Caserta, Italy

Abstract

Telomere length maintenance ensures self-renewal of human embryonic stem cells (hESCs) and induced pluripotent stem cells (iPSCs), however the mechanisms governing telomere length homeostasis in these cell types are unclear. Here, we report that telomere length is determined by the balance between telomere elongation mediated by telomerase and telomere trimming, controlled by the homologous recombination proteins XRCC3 and Nbs1 that generate single-stranded C-rich telomeric DNA and double-stranded telomeric circular DNA (T-circles), respectively. We found that reprogramming of differentiated cells induces T-circle and single stranded C-rich telomeric DNA accumulation, indicating the activation of telomere trimming pathways that compensate telomerase dependent telomere elongation in hiPSCs. Excessive telomere elongation compromises telomere stability and promotes the formation of partially single-stranded telomeric DNA circles (C-circles) in hESCs, suggesting heightened sensitivity of stem cells to replication stress at overly long telomeres. Thus, tight control of telomere length homeostasis is essential to maintain telomere stability in hESCs.

Introduction

Telomeres are nucleoprotein structures at the end of linear chromosomes that consist of tandem TTAGGG repeats, bound by the shelterin complex[1]. They are characterized by single-stranded (ss) terminal overhangs, known as G-tails[2]. The G-overhang can invade the double-stranded (ds) telomeric region forming a stable secondary structure called the T-

*To whom correspondence should be addressed: Karlseder@salk.edu.

Author Contributions

T. R. designed and performed the experiments and wrote the manuscript. C.H. carried out experiments. S.C. provided the G-quadruplex ligand RHPS4. J.K. designed experiments, supervised the work and wrote the manuscript.

Competing Financial Interest Statement:

I declare that the authors have no competing financial interest as defined by Nature Publishing Group, or other interests that might be perceived to influence the results and discussion reported in this paper.

Data availability statement:

The authors declare that [the/all other] data supporting the findings of this study are available within the paper and its supplementary information files.

loop[3], a conserved protective structure that prevents the chromosome ends from being recognized as DNA damage[4,5].

During each cell division telomeres shorten due the 'end-replication problem'[6,7], as well as telomere end processing[8]. Telomere shortening can be counteracted by lengthening mechanisms. The majority of cancer cells, cells of the germ line and stem cells activate the ribonucleoprotein enzyme telomerase to compensate for telomere loss[9,10]. The telomerase core-complex consists of the reverse transcriptase hTERT and the RNA component hTR, used as a template to synthesize telomeric DNA[11]. Alternatively, a fraction of human cancer cells maintain telomere length by telomerase-independent mechanisms, referred to as alternative lengthening of telomeres (ALT)[12]. ALT cells rely on recombination pathways, showing high incidence of telomere sister chromatid exchange events (t-SCE)[13] and a number of distinctive characteristics, such as ALT-associated promyelocytic leukemia (PML) bodies (APBs) containing telomeric chromatin[14], heterogeneous telomere length[15], elevated levels of 5′ C-rich telomeric overhangs[16] and abundance of extrachromosomal telomeric repeats (ECTR), including linear ds DNA[17], ds telomeric circles (T-circles)[18] and partially ss circles (C-circles)[19]. However, whether accumulation of ALT related telomeric features is restricted to ALT activity is still under debate.

Telomere length homeostasis dictates cellular proliferative potential and becomes determinant in stem cells, where it ensures tissue homeostasis and impacts on age-related deterioration of stem cell function[20]. During embryogenesis, telomere length is established such that long telomeres can support extended series of regulated cells divisions during the developmental program, but short enough to limit cell proliferation in the adult to suppress cancer initiation[21]. The stable telomere length found in human embryonic stem cells (hESCs)[22], suggests that defined mechanisms have evolved to promote the optimal telomere length that ensures genomic stability.

Telomere length maintenance has also become of special interest for the reprogramming of somatic cells, as it directly impacts on reprogramming efficiency and determines the maintenance of the pluripotent phenotype[23].

Here we aimed to gain insight into the mechanisms controlling telomere length homeostasis in hESCs and hiPSCs. We reveal that in addition to telomerase-dependent telomere elongation, active telomere trimming mechanisms regulate telomere length. We demonstrate that XRCC3 and Nbs1 mediate telomere attrition by catalyzing the formation of T-circles and C-rich overhangs. Moreover, hESCs accumulate other hallmarks of ALT, such as C-circles, as a result of increased telomere instability, but independent of recombination-mediated telomere elongation. We show that reprogramming of human differentiated cells leads to the appearance of C-rich overhangs and ECTR in hiPSCs, which represents a valuable marker to characterize reprogramming efficiency. Our results demonstrate that the fine balance between telomere length control pathways dictates telomere stability in pluripotent stem cells, which is essential for our understanding of stem cell biology for stem cell based therapies.

Results

Cytosine-rich telomeric overhang and extrachromosomal telomeric repeats in hESCs

C-rich overhangs of 3′-5′ orientation were initially related to ALT activity[16,24], however, some telomerase positive human cancer cells with over-elongated telomeres[25] and cells of germ line origin[26] also accumulate ss C-rich telomeric DNA. To evaluate C-rich overhang in hESCs, we performed native and denaturing two-dimensional (2D) gel electrophoresis on DNAs from three different hESC lines (HUES6, H1 and H9), enabling the separation of restriction fragments (TRFs) by size and structure[18,27,28] (Fig. 1a). 2D analysis revealed G-rich ss telomeric DNA under native conditions (Fig. 1b, top panel) that resembled the arc corresponding to ds telomeric DNA under denaturing conditions. In-gel hybridizations using a G-rich probe allowed us to detect C-rich ss telomeric DNA of equivalent intensity to the canonical G-overhang that also followed the same path as the ds telomeric DNA under denaturing conditions, indicating C-rich overhangs in HUES6 cells (Fig. 1b, lower panels). We also observed ss C-rich telomeric DNA in H1 and H9 cell lines consistent with the presence of 5′ C-overhang in hESCs (Supplementary Fig. 1a, right panels).

To confirm the polarity of both overhangs, we treated the samples with ss DNA-specific exonucleases Exonuclease 1 (Exo1), with 3′-5′ polarity, or RecJf, with 5′-3′ polarity, prior to DNA restriction digestion. G-overhangs were susceptible to Exo1 treatment but resistant to RecJf. C-overhangs were only sensitive to RecJf digestion (Fig. 1b). Thus, our results indicate terminal ss C-rich DNA with 3′-5′ orientation at telomeres in hESCs.

Ds circular telomeric DNA in the form of T-circles was clearly visible with both strand-specific telomeric probes under denaturing conditions in the three hESC lines (Fig. 1b and Supplementary Fig. 1a, red arrows).

To further explore the presence of circular C-rich partially ss ECTR (C-circles) we performed C-circle assays[19] in hESCs (Fig. 1c). We included samples from ALT cells (U2OS) as a positive control and human primary fibroblast (IMR90) as negative control. As expected, C-circles were abundant in U2OS cells and absent in IMR90 cells. Strikingly, all hESC lines showed significantly higher levels of C-circles compared with IMR90 cells (Fig. 1d), indicating the presence of circular C-rich partially ss ECTR in hESCs.

Considering that C-overhangs and ECTR, in particular C-circles, are distinctive characteristics of ALT cells[19], we investigated whether hESCs employ ALT mechanisms for telomere elongation. Telomere recombination was evaluated by Chromosome-Orientation-FISH (CO-FISH) analysis on metaphase chromosomes[13] (Fig. 2a). We detected very low rates of t-SCE in hESCs, compared to the high frequency observed in ALT cells (U2OS) (Fig. 2a). Thus, to test whether telomere recombination contributes to telomere elongation pathways, we generated hESCs with reduced telomerase activity through the expression of dominant negative hTERT (Fig. 2b). These cells progressively shortened telomeres (Fig. 2c), indicating that telomere recombination could not compensate for impaired telomerase activity. Similarly, we did not observe ALT-associated PML bodies (APB) in hESCs (Supplementary Fig. 1b). We conclude that despite the presence of a subset of ALT markers, hESCs do not rely on telomere recombination mechanisms for elongation.

Excessive telomere elongation in hESCs leads to the accumulation of ECTR without altering the frequency of t-SCE events

To understand the mechanism of ECTR formation in hESCs, we asked whether ECTR accumulation is associated with telomerase-mediated telomere lengthening. Overexpression of the RNA component (hTR) (Supplementary Fig. 2a) led to a significant increase in telomerase activity (Supplementary Fig. 2b) and rapid telomere elongation in HUES6+hTR cells (Fig. 3a). Elongated telomeres became homogeneous in length with continuous culture (Fig. 3b) and hESCs maintain stem cell renewal capacity (Supplementary Fig. 2c) and differentiation potential into germ layers (Supplementary Fig. 2d,e). Thus, hESCs can establish a new telomere length set point when telomerase activity increases. To determine whether telomere elongation promotes accumulation of ss telomeric repeats, we performed TRF analysis under native and denaturing conditions using a C-rich or G-rich telomeric probe. We found that over-lengthened telomeres present similar ratio of G- and C-tails, suggesting that the number of telomeres bearing 3′ G- and 5′ C-overhang is maintained (Fig. 3b).

In addition, we evaluated T-circle and C-circle production in hESCs with over-elongated telomeres. T-circle assays demonstrated a significant increase in T-circle formation relative to control cells (Fig. 3c). Excessive telomere elongation also generated a robust accumulation of C-circles (Fig. 3d). Given that long telomeres emerged as a requirement for ALT induction[29], we investigated whether severe telomere elongation in hESCs facilitates the activation of ALT. CO-FISH analysis showed that t-SCE rates was similar in control and hTR overexpressing cells (Fig. 3e). Secondly, we did not observe APB-like foci. We conclude that telomerase-dependent elongation generates a subset of ALT hallmarks in hESCs, independently of ALT activation.

Reprogramming of differentiated human cells induces the accumulation of 5′ C-rich telomeric overhangs and ECTR

We next asked whether the features identified for hESCs could be induced by reprogramming of differentiated cells, which lack these characteristics. We generated iPS cell lines by retroviral transduction of primary human lung fibroblast (IMR90) with Oct4, Sox2, Klf4 and c-Myc. We confirmed the activation of endogenous pluripotent factors (Supplementary Fig. 3a–c) and performed functional analysis by differentiation into the embryonic germ layers *in vitro* (Supplementary Fig. 3d,e).

To ascertain whether the generated iPSCs acquired the same characteristics as hESCs, we analyzed DNA isolated from three different iPSC lines by 2D gel electrophoresis. Hybridization with a G-rich and C-rich probe under native and denaturing conditions showed the presence of G- and C-overhangs, whereas only G-overhangs were detected in the parental fibroblasts (Fig. 4a). T-circles were clearly visible with both strand-specific probes under denaturing conditions but not in the parental cells (Fig. 4a, red arrows), indeed the levels detected in the iPSCs were comparable to those observed in hESCs (Supplementary Fig. 4a).

We then examined the presence of C-circles in iPSCs. Reprogramming induced C-circles similarly to the levels detected in hESCs (Fig. 4b). Since we found hallmarks of ALT cells in iPSCs and considering that several groups observed telomere elongation in iPSCs derived from telomerase deficient cells[30–32], we evaluated the contribution of telomere recombination mechanisms for telomere elongation in iPSCs. We observed very low t-SCE frequencies in both the parental cells and the iPSCs, in contrast to the high frequency detected in U2OS cells (Fig. 4c). We did not detect APB in these cells (Supplementary Fig. 4b), demonstrating that reprogramming of differentiated cells generates 5′ C-rich overhangs and ECTR without the activation of homologous recombination-mediated telomere maintenance, supporting our findings in hESCs.

We found quantitatively comparable levels of telomerase activation between hESCs and iPSC lines, as well as iPSC lines derived from HUVEC and keratinocytes[33,34] (Supplementary Fig. 4c). Moreover, TRF analysis revealed that iPSCs acquired a similar telomere length setting as hESCs (Supplementary Fig. 4d), suggesting that the reprogrammed cells activate telomere length homeostasis pathways.

To investigate the impact of telomerase activation and telomere elongation on the formation of ECTR, we examined T and C-circle formation in IMR90 cells expressing telomerase (Supplementary Fig. 5a). Elongation of telomeres induced rapid accumulation of T-circles at increasing population doublings (PD) (Supplementary Fig. 5b,c). C-circles were not detected at early PDs but only when telomeres became very long (Supplementary Fig. 5d). Elongation of telomeres has a stronger impact on C-circle formation in hESCs (Fig. 3d) than in IMR90 cells, suggesting that additional factors contribute to C-circle accumulation in hESCs.

Replicative stress causes accumulation C-circles in hESCs

Recent studies demonstrated the correlation between DNA replication stress and C-circle formation[29,35]. To investigate the origin of C-circle accumulation in hESCs we treated hESCs with long telomeres with different doses of the replication stress inducing drugs hydroxyurea (HU) and aphidicolin (Aph) for 24 hours, and C-circle formation was ascertained (Fig. 5a). Exposure to high doses of HU (3 mM) or Aph (5 μM) reduced DNA replication activity (Supplementary Fig. 6a) followed by increased accumulation of C-circles (Fig. 5a). A significant accumulation of C-circles was also detected in HUES6-vector cells subjected to replication stress, however the levels remained lower compared to HUES6+hTR treated cells, suggesting that long telomeres are prone to suffer more replication defects.

To confirm that defective telomere replication triggers C-circle formation in hESCs, cells were treated with the G-quadruplex (G4) ligand, RHPS4, previously reported to interfere with telomere replication[36]. Flow cytometry showed deficient S-phase progression after the treatment (Supplementary Fig. 6a) followed by a similar increase of C-circle levels, as did the treatment with DNA replication inhibitors (Fig. 5a), supporting the idea that replication defects are a major cause for C-circle accumulation in hESCs.

To gain insight into the molecular mechanisms underlying C-circle formation in hESCs, we examined the contribution of factors that have previously been implicated in C-circle

production: TRF1, the RECQ helicases BLM and WRN, Exonuclease 1 (Exo1), the helicase/nuclease DNA2 and a member of the SNF2 family of DNA-dependent ATPases, SMARCAL1[29,35]. Cells depleted of TRF1, BLM, WRN or Exo1, exhibited similar amounts of C-circles as control cells. In contrast, DNA2 and SMARCAL1-deficient cells accumulated significantly more C-circles (Fig. 5b and Supplementary Fig. 6b). DNA2 has an essential role preventing telomere replication defects by resolving G4 structures[37] and promoting degradation of reversed replication forks after fork stalling[38]. SMARCAL1 catalyzes fork regression and is required for successful replication through telomeric sequences[35]. Thus, we speculate that accumulation of G4 structures and aberrant processing of unresolved replication intermediates within telomeres upon DNA2 or SMARCAL1 depletion drives the accumulation of C-circles. Since this effect is exacerbated in cells with long telomeres, we reasoned that long telomeric tracks could be prone to accumulate more replication stress. We tested whether hESCs with long telomeres displayed fragile telomere phenotypes arising from telomeric DNA replicative defects[39]. We observed higher frequencies of metaphase chromosomes with multi-telomeric signals (MTS) in cells with overextended telomeres (Fig. 5c), indicating increased replication defects.

To determine whether telomerase plays a role during telomere replication, we subjected hESCs to TERT knockdown (Supplementary Fig. 6c) and assessed the frequency of MTS. TERT-deficient cells exhibited comparable levels of MTS as control cells in both hESCs and hESCs with very long telomeres (Supplementary Fig. 6d), demonstrating that the presence of over-elongated telomeres rather than changes in telomerase expression led to telomere fragility. Likewise, these cells accumulated a significant number of telomere dysfunction-induced foci (TIFs) (Fig. 5d), indicating that excessively long repetitive sequences compromise telomere stability. We observed that telomere elongation is followed by augmented loading of telomeric proteins (Supplementary Fig. 6e) suggesting that the slight increase in TIFs is likely due to DNA replication defects rather than defective telomere capping.

These data suggest that tight control of telomere length homeostasis is required to prevent telomere fragility and DNA damage at telomeres in hESCs, ensuring telomere integrity and maintenance of genome stability.

XRCC3 and Nbs1 contribute to the formation of 5′ C-rich telomeric DNA and T-circles

We next investigated the molecular mechanisms underlying 5′ C-rich overhang formation and T-circles in hESCs. Human 5′ C-rich telomeric overhangs have been proposed to accumulate in the context of T-loop resolution events mediated by XRCC3[40]. To evaluate the contribution of XRCC3 in overhang formation in hESCs, we suppressed XRCC3 and performed native TRF analysis (Fig. 6a and Supplementary Fig. 7a). The G-overhang signal was not significantly altered, however we detected a 40% reduction in the levels of C-overhangs. Thus, these results support a highly conserved role for XRCC3 in C-overhang generation.

XRCC3 has been implicated in T-circle formation in different scenarios[26,28,41]. However, we did not find a significant effect on T-circle accumulation in hESCs (Supplementary Fig. 7b), suggesting that XRCC3 activity is not sufficient to promote T-circle formation there. We

then focused on Nbs1, a member of the Mre11/Rad50/Nbs1 complex and potential candidate involved in T-Circle formation[28,41]. Nbs1 knockdown to approximately 45% and 25% relative to control cells preserved stem-cell renewal capacity of hESCs (Supplementary Fig. 7c,f). Nbs1 depleted cells exhibited a significant reduction of T-circles (Fig. 6b), and we therefore suggest that Nbs1 is at least partly responsible for T-circle accumulation in hESCs.

It has been hypothesized that T-circles and C-overhangs could act as the precursors of C-circles[16,42]. Since our data demonstrated a direct role of XRCC3 and Nbs1 in C-overhang and T-circle formation respectively, we evaluated the accumulation of C-circles in the absence of these factors, but we did not observe changes in C-circle abundance (Supplementary Fig. 7d,e). Thus, we conclude that different pathways contribute to the generation of both types of ECTR in hESCs.

XRCC3 and Nbs1 regulate telomere length in hESCs

Our findings indicate that formation of 5′ C-rich overhangs and T-circle generation depends on XRCC3 and Nbs1. If these structures accumulate in hESCs as an outcome of processing events at the chromosome ends, depletion of XRCC3 and Nbs1 should result in telomere length changes. We evaluated telomere length 7 days after transduction of siRNAs or shRNAs for single and double depletions (Supplementary Fig. 7f). While the single knockdown of XRCC3 or Nbs1 did not significantly modify the distribution of the telomeric signal, cells with reduced levels of both factors showed telomere lengthening (Fig. 6c), indicating defective telomere trimming. These data strongly suggest that XRCC3 and Nbs1 mediate telomere length regulation through partially distinct parallel pathways and influence telomere length homeostasis in hESCs.

In summary, our results demonstrate that telomere length regulation in hESCs is mediated by telomerase-dependent elongation and by the HR factors XRCC3 and Nbs1 that counteract excessive telomere elongation. We hypothesize that the activation of telomere trimming events involves the resolution of the T-loop into a T-circle and ss C-rich telomeric DNA. We observed that telomere length homeostasis is crucial to prevent telomere instability in hESCs. We establish that reprogramming of differentiated cells induces the accumulation of T-circle and ss C-rich telomeric DNA, indicating the activation of telomere trimming pathways and emphasizing the requirement of tight telomere length homeostasis for telomere stability in hESC and iPSC.

Discussion

We have discovered that hESCs tightly control telomere length by establishing a proper equilibrium between elongation and trimming. Telomere elongation is achieved by telomerase while counteracted by HR factors that promote the generation of C-rich ss telomeric DNA and ECTR in the form of T-circles. Failure in maintaining length homeostasis leads to telomere instability and accumulation of C-circles. These features are also acquired by reprogramming of human somatic cells, therefore we suggest that such characteristics represent reliable markers for pluripotency.

Telomere elongation in hESCs and iPSCs

The contribution of telomerase independent telomere maintenance pathways in stem cell populations remains controversial. Initial studies in telomerase deficient mESCs showed telomere length maintenance in long-term cultures of proliferative survivors[43]. High frequency of t-SCEs was observed in telomerase deficient mESCs[44] and telomere recombination was proposed to compensate the loss of telomerase in mESCs[45]. In contrast, our data suggest that telomere elongation in hESCs is exclusively mediated by telomerase and recombination dependent pathways are not activated when telomerase activity is reduced. Consistently, a recent study showed that telomerase deficient hESCs exhibited progressive telomere shortening in continuous culture, concomitant with reduced proliferation and increased cell death[46]. Likewise, while studies in miPSCs derived from telomerase-deficient mice suggested the contribution of ALT pathways for telomere maintenance[30,32], ALT activity was not detected in telomerase-mutant hiPSCs[47], consistent with our model. Analysis of hiPSCs derived from patients with telomere shortening disorders revealed that the severity of telomere elongation defects correlated with the degree of telomerase deficiency[47–49]. We observed comparable telomerase expression levels and telomere length between hiPSCs derived from different sources of primary cells that also resembled those detected in hESCs. However, variability in telomerase expression and telomere elongation has been reported among hiPSC clones, suggesting that hiPSCs are not homogeneous clonal populations and culture conditions impact on telomerase expression and function[47]. We propose that not only telomerase activity regulates telomere length, but also trimming mechanisms directly contribute to the proper telomere length set-point. We suggest that future studies of the components that dictate telomere length homeostasis will facilitate the development of stem cell based therapies for telomere biology disorders.

XRCC3 and Nbs1 regulate telomere length in hESCs

The accumulation of ECTR in the form of T-circles after excessive telomere elongation indicated the activation of telomere trimming events in hESCs. Telomere length control by trimming involves the conversion of a T-loop into a T-circle and a 5′ C-rich ss telomeric DNA intermediate[26]. According to our results, the maintenance of the ratio between G- and C-rich ss telomeric DNA after telomere elongation suggests that telomere deletion events are followed by nuclease degradation that compensates for the excess of 5′ C-rich ss telomeric DNA, indicating the presence of tightly controlled regulation of the balance between the overhangs. Given that previous *in vitro* studies demonstrated that G- and C-rich overhangs are equally efficient for the invasion of the duplex telomeric DNA[50], it would be of special interest to investigate whether they are both implicated in the formation of a protective structure at telomeres in hESCs and hiPSCs.

Resolution of the T-loop as a Holliday junction by HR is mediated by Nbs1 and XRCC3[28]. Nbs1 also regulates telomere length in ALT cells through recombination-mediated telomere elongation[51]. However, only XRCC3 was reported to contribute to telomere trimming pathways in telomerase positive cancer cells[26]. Our results are consistent with a synergistic role of XRCC3 and Nbs1 in hESCs as major regulators of telomere length by trimming mechanisms based on T-loop resolution. Therefore, when telomeres are elongated beyond a threshold, XRCC3 mediates C-rich ss telomeric DNA processing and Nbs1 promotes the

resolution of T-circles (Fig. 7a,b). We cannot exclude that both XRCC3 and Nbs1 contribute to the formation of C-rich ss telomeric DNA and T-circles. Therefore complete deletion of these factors may be necessary to address this question, however, loss of HR factors leads to embryonic lethality, reduced growth rate and increased cell death[52,53], hindering the analysis.

The presence of trimming pathways in hESCs suggests that excessive telomere elongation could compromise genome integrity. Telomeres are known to be fragile sites prone to accumulate stalled replication forks[39] and secondary structures, including G-quadruplexes, challenging DNA replication[54]. Furthermore, telomere replication stress could promote genome instability and cancer[55]. Our data indicate that hESCs with long telomeres exhibit increased telomeric DNA damage likely due to augmented telomere replication stress. Since the number of dysfunctional telomeres in cancer cells does not increase following excessive telomere elongation[25], these results suggest that hESCs harbor more stringent mechanisms to sense inappropriate telomere replication, since the maintenance of telomere stability is of critical importance to assure tissue homeostasis and prevent cancer development. We also propose that tight regulation of telomere trimming mechanisms exist in hESCs to prevent excessive telomere attrition that could compromise their pluripotent potential and contribute to the age-related deterioration in stem cell function[20].

Replication stress causes C-circle accumulation in hESCs

The elevated frequency of t-SCEs and the presence of C-circles were considered the best indicators for ALT[13,19]. Nevertheless, a recent study demonstrated the induction of C-circles in telomerase positive cancer cells upon depletion of SMARCAL1, which led to telomere replication stress. No other ALT-related phenotypes were induced[35]. The first observation of C-circle accumulation in response to perturbations in DNA replication was reported in telomerase positive cancer cells due to defective chromatin assembly following depletion of the histone chaperone ASF1. ALT activity was activated and C-circle levels reached the amount detected in ALT cells[29]. Therefore, it is conceivable that C-circle levels beyond a threshold may be indicative of ALT. Our data also support this hypothesis, as the amount of C-circles detected in hESCs was not as high as that seen in U2OS cells, consistent with the lack of ALT activity in hESCs. Elongation of telomeres caused a dramatic increase in C-circle abundance, likewise, the aforementioned phenotypes were observed in cells with very long telomeres[29,35]. We propose that telomere length determines the formation of these telomeric DNA structures and that replication stress, which is exacerbated in the presence of long telomeres, triggers their accumulation (Fig. 7c). Consistently, we show an increase of C-circles following DNA replication stress in hESCs, suggesting that severe abrogation of DNA replication activity boosts C-circle formation. Remarkably, C-circle metabolism might differ between cell types, since treatment with DNA replication inhibitors has a different effect in cancer cells[29]. Supporting our data, we show that depletion of DNA2 and SMARCAL1 led to elevated C-circle accumulation consistent with their active role in S-phase progression, likely by facilitating repair and restart of stalled replication forks[38,56].

While the molecular mechanism governing C-circle formation remains elusive, we suggest that very long telomeres trigger C-circle accumulation. The increased telomere instability

observed in this scenario results in C-circle generation as byproduct of telomeric DNA replication intermediates resolution. Excessive experimental telomere elongation in primary fibroblasts also induced C-circle accumulation, albeit to a much lesser extent compared to hESCs with long telomeres. We did not detect changes in the levels of ss C-rich linear telomeric DNA following replication stress, demonstrating that resolution of replication intermediates specifically enriches for C-rich telomeric DNA in circular conformation. We suggest that hESCs accumulate higher levels of replication stress compared to differentiated cells, which is consistent with the demonstration that replication intermediates are frequently observed in ESC, but lost after differentiation[57].

Altogether our study establishes that a very tight control of telomere length homeostasis, regulated by telomerase-dependent elongation and telomere trimming events, is required to ensure telomere stability in hESCs. This balance is also established in hiPSCs, providing novel insights into the characterization of faithfully reprogrammed cells, which represent the most attractive tool in regenerative medicine due to their therapeutic potential.

Methods

Cell lines

Human H1 (WA01) and H9 (WA09) embryonic stem cell lines were obtained from WiCell Research Institute and HUES6 from Harvard. Human diploid IMR90 fibroblasts were obtained from ATCC. hESCs and iPSCs were maintained on a mitotically inactive mouse embryonic fibroblast (MEFs, Millipore) feeder layer in hES medium, DMEM/F12 (Invitrogen) supplemented with 20% Knockout Serum Replacement (Invitrogen), 1 mM L-glutamine, 0.1 mM non-essential amino acids, 55 μM β-mercaptoethanol and 10 ng/ml bFGF (Joint Protein Central). hESCs and iPSCs were also cultured in Matrigel (BD Biosciences) using mTeSR [59].

Human diploid IMR90 fibroblasts were cultured in Glutamax-DMEM (Life Technologies) supplemented with 15% FBS and 0.1 mM non-essential amino acids. U2OS and 293T cells were cultured in Glutamax-DMEM (Invitrogen) supplemented with 10% FBS and 0.1 mM non-essential aminoacids at 7.5% CO_2 and 3% O_2.

For differentiation into embryoid bodies (EBs), pluripotent cell colonies growing on MEFs were loosely detached by dispase treatment, resuspended in DMEM/F12 supplemented with 10% FBS (Invitrogen), 0.5 mM L-glutamine, 0.1 mM non-essential amino acids and maintained on low attachment plates for 4 days. The EBs were then plated on gelatin-coated plates and allowed to differentiate for another 10 days.

Human iPSC generation

IMR90 fibroblasts were infected with an equal ratio of retroviruses encoding Oct4, Klf4, Sox2 and c-Myc by spinfection at 800xg for 1 hour at room temperature in the presence of polybrene (4 μg/ml). Cells were passaged onto fresh MEFs and switched to hES cell medium 4 days after the infection. For the derivation of hiPS cell lines, colonies were manually picked and transferred onto MEF feeder cells for several passages before growth in Matrigel/mTeSR conditions.

Cytogenetics

Cells were sent to Cell Line Genetics (Madison, WI) for routine karyotype analysis.

Plasmids and virus preparation

pMX-Oct4, pMX-SOX2, pMX-KLF4, pMX-cMyc were obtained from Addgene (plasmids 17217, 17218, 17219, 17220 respectively). Retroviral vectors were co-transfected with packaging plasmids (pCMV-gag-pol-PA and pCMV-VSVg, kindly provided by Gerald Pao, Laboratory of Genetics, The Salk Institute, La Jolla, CA) in 293T cells using Lipofectamine (Invitrogen) in accordance with manufacturer's recommendations.

pBABE-U3-hTR was kindly provided by Kathleen Collins[60]. U3-hTR was cloned into third generation lentiviral vector kindly provided by Raul Alvarez Rodriguez (Laboratory of Genetics, The Salk Institute, La Jolla, CA). pBABE-TERT and TERT-DN[61] were subcloned into pLV-FU-TetO vector. Lentiviral vectors were co-transfected with packaging plasmids (pMDL, Rev and VSVg, kindly provided by Oded Singer, Laboratory of Genetics, The Salk Institute, La Jolla, CA) in 293T cells using Lipofectamine (Invitrogen) in accordance with manufacturer's recommendations.

Lentiviral supernatants were collected 36 hours after transfection, concentrated by ultracentrifugation at 19400 rpm for 2 hours and resuspended in hES cell media.

The shRNA-expressing lentiviral pLKO.1 vectors were purchased from OpenBiosystems (ThermoFisher) and correspond to the following clones:

shTERT: TRC180780; Nbs1 sh1: TRC40135; Nbs1 sh2: TRC40137; pLKO.1 scramble shRNA (sense sequence 5′-CCTAAGGTTAAGTCGCCCTCG-3′)[62].

Viral particles were produced in the Salk Viral Core using standard protocols.

Lentiviral infections of hESCs were performed as previously described [63].

siRNA transfections and treatments

HUES6 cells were transfected using Lipofectamine RNAiMAX (ThermoFisher) transfection reagent according to the manufacturer's recommendations. ON-TARGET*plus* SMART pool of four siRNAs from Dharmacon (ThermoFisher) were used for siRNA knockdown: TRF1 (catalogue #L-010542-02-0005); BLM: (catalogue #L-007287-00-0005); WRN: (catalogue #L-010378-00-0005); Exo1: (catalogue #L-013120-00-0005); DNA2: (catalogue #L-026431-01-0005); SMARCAL1: (catalogue # L-013058-00-0005); XRCC3: (catalogue # L-012067-00-0005) or control non-targeting pool (catalogue # D-001810-10-20). The cells were collected 72 h or 96 h post treatment after two serial transfections and processed for protein, RNA and DNA analyses.

Cells were treated with 0.2mM or 3mM hydroxyurea (Sigma), 5μM aphidicolin (AG Scientific) or 0.5μM RHPS4 for 24h, and collected for DNA analysis.

RNA Isolation and Real-Time PCR Analysis

RNA was extracted with Trizol Reagent (Invitrogen) according to manufacturer's instructions and purified using RNeasy mini kits (Qiagen). cDNA was synthesized using the Superscript III Reverse Transcriptase kit (Life Technologies) and qRT-PCR was performed using the SYBR Green master mix (ABI, Life Technologies). Values of gene expression were normalized using GAPDH expression and are shown as fold change relative to the value of the sample control. The list of the primers used in the RT-PCR analysis is provided in the Supplementary Table 1.

Chromatin immunoprecipitation (ChIP)

ChIP was performed as described by[50].

Immunofluorescence and telomere FISH on metaphase spread

Cytocentrifugation, immunofluorescence and telomeric FISH were carried out as described[64]. For metaphase analysis, ≥ 25 metaphases were quantified for each metaphase-TIF experimental replicate.

Immunofluorescence

Immunostainings were performed as described[63]. Antibodies used for immunofluorescence: TRF2 (Genlantis ABI124); PML (sc-5621); Sox2 (Chemicon 5603); SSEA4 (ab16287); Oct4 (cell signaling 2750); TRA-1-60 (MAB4360); AFP, anti-alpha-1-fetoprotein (Dako A0008); SMA, anti-actin α-smooth muscle (Sigma A5228); TUJ1, anti tubulin β3 (Covance, MMS-435P); Cdx2 (Dako M3636).

Chromosome orientation FISH

CO-FISH was performed as described previously[29]. Metaphase chromosomes were visualized by conventional fluorescence using a 63X objective lens on a Zeiss Axioplan II microscope and ≥ 25 metaphases were analyzed in each experimental replicate.

Native and denaturing in-gel hybridization

Telomere restriction fragments were analyzed as described[65], briefly, genomic DNA was purified, digested with *Alu*I and *Mbo*I (New England Biolabs), and separated by gel electrophoresis on 0.6% agarose gels at 100 V for 1 h then 38 V overnight in 0.5X TBE buffer. After electrophoresis DNA was stained with ethidium bromide in 0.5X TBE buffer and the gels were dried at 50°C for 3 h, and hybridized with a ^{32}P-end-labeled $(TTAGGG)_4$ oligo probe. After imaging, gels were denatured, neutralized and rehybridized as described above. Gels were exposed using PhosphoImager screens, scanned in a Typhoon 9400 PhosphoImager (Amersham, GE Healthcare) and analyzed using ImageQuant Software.

Two-Dimensional Gel Electrophoresis

2D analysis was carried out as described[18,24].

C-circle assay

The method employed for the assay probing for C-circles was slightly modified from that performed in Henson et al.[19]. Briefly, genomic DNA was prepared as above. Digested DNA was cleaned up by phenol-chloroform extraction and precipitation. DNA was diluted and measured using a Nanodrop spectrophotometer. Generally, 100 and 50 ng of DNA were used for each sample (10 μl). DNA was combined with 10 μl 0.2 mg/ml BSA (NEB), 0.1% Tween, 1 mM each dATP, dGTP and dTTP, 1X ϕ29 Buffer (NEB) and 7.5 U ϕ29 DNA polymerase (NEB) and incubated at 30 °C for 12 h then 65 °C for 20 min. Reaction products were diluted to 100 μl with 2XSSC and dot-blotted onto a 2XSSC soaked nylon membrane. DNA was UV-cross-linked onto the membrane, and then hybridized at 50°C with end-labeled ^{32}P-$(CCCTAA)_4$ oligo probe. Blots were washed, exposed and scanned using a Typhoon 9400 PhosphoImager (Amersham, GE Healthcare) and analyzed using ImageQuant Software.

T-circle assay

T-circle assay was conducted as described[40,66].

Flow cytometry analysis

For cell cycle analysis, HUES6 cells were individualized using accutase 1:4 in PBS and fixed in 70% ethanol overnight. For BrdU detection, cells were incubated with 10 μM BrdU for 30 minutes before collection. After incubation with 0.5 mg/ml pepsin cells were treated with 2 N HCl for 20 minutes, washed and incubated with a rat-antiBrdU antibody (AbD serotec) for 45 minutes followed by incubation with goat anti-rat-FITC secondary antibody (Southern Biotech) for 30 minutes. Cells were then resuspended in PBS containing 50 μg/ml of propidium iodide and 0.5 mg/ml of RNaseA. Flow cytometry analyses were conducted using a LSRII cytometer (BD Bioscience) and data was analyzed using FlowJo software.

Telomerase assay

Telomerase activity was analyzed by PCR-based telomeric repeat amplification assay. hESCs were collected in cold PBS. Cell pellets were resuspended in telomerase buffer (TB) (10 mM Tris pH 8.5, 3 mM KCl, 1 mM $MgCl_2$, 1 mM DTT) containing protease and RNase inhibitors. Cells were incubated in TB buffer on ice for 15 to 20 minutes and lysis was monitored taking small aliquots under the microscope. Cytoplasmic extracts were collected by centrifugation, adjusted to 20% glycerol and 0.1 M NaCl, aliquoted and stored at −80°C. Protein concentration was determined and cytoplasmic extracts were diluted accordingly with TB containing 10% glycerol, protease and RNase inhibitors.

Telomerase elongation reaction was performed using different concentrations of extracts. The diluted extract was added to the elongation mix containing 0.1 mM each dATP, dGTP, dTTP, 0.25 mM Spermidine, 25 μM Spermine, 5 mM $MgCl_2$ and 17.5 ng/μl of primer (GCACATGCATCGAGAGTT) in TB and incubated during 30 minutes at 30°C. A mix of proteinase K, SDS, Tris-CDTA was added to stop the reaction and incubated 1 h at 37°C. After addition of 0.2 M LiCl, the reaction was extracted with phenol-chloroform and precipitated in ethanol overnight. Pellets were resuspended in 10 mM Tris pH8 and incubated with the PCR reaction mix: 1.5 mM $MgCl_2$, 0.2 mM each dATP, dGTP, dTTP,

2.5μM dCTP, 0.125 μl ^{32}P dCTP, 0.55 μl primary primer (GCACATGCATCGAGAGTT), 0.55 μl secondary primer (CGACTTGCCTAACCCTAA) and 0.2 μl AmpliTaq (Life Technologies) in Amplitaq buffer. Amplification reaction was carried out in a thermal cycler as follows: 4 min at 94°C followed by 29 cycles of PCR reaction (94°C for 30 s, 55°C for 1 min, 72°C for 1 min) and 5 min at 72°C. The amplified product was analyzed in 8% acrylamide-urea denaturing gel. The gel was dried at 75°C for 1h and exposed to PhosphoImager screen overnight, scanned in a Typhoon 9400 PhosphoImager (Amersham, GE Healthcare) and analyzed using ImageQuant Software.

Statistical methods

All statistical analysis was performed using Prism 6 software. The number of independent experiments analyzed is shown in each figure legend. The significance between means was determined with a two-tailed unpaired Student's t test when Gaussian distribution was assumed and two-tailed Mann-Whitney test when not assumed. Statistically significant values are depicted as follows: ****$P < 0.0001$, ***$P < 0.001$, **$P < 0.01$ *$P < 0.05$; NS, not significant.

Supplementary Material

Refer to Web version on PubMed Central for supplementary material.

Acknowledgments

We are grateful to K. Collins (University of California, Berkeley, California) for generously sharing the pBABE-hTR plasmid and R. Alvarez Rodriguez (The Salk Institute, La Jolla, California) and the Belmonte laboratory (The Salk Institute, La Jolla, California) for sharing reagents. We thank the members of the Salk Institute's Stem Cell Core (La Jolla, California) for expert advice and the Karlseder laboratory for comments. T.R. was supported by the Glenn Center for Research on Aging and CIRM training grant TG2-01158. The Salk Institute Cancer Center Core Grant (P30CA014195), the NIH (R01GM087476, R01CA174942), the Donald and Darlene Shiley Chair, the Highland Street Foundation, the Fritz B. Burns Foundation, the Emerald Foundation and the Glenn Center for Aging Research support J.K.

References

1. de Lange T. Shelterin: the protein complex that shapes and safeguards human telomeres. Genes Dev. 2005; 19:2100–10. [PubMed: 16166375]
2. Makarov VL, Hirose Y, Langmore JP. Long G tails at both ends of human chromosomes suggest a C strand degradation mechanism for telomere shortening. Cell. 1997; 88:657–66. [PubMed: 9054505]
3. Griffith JD, et al. Mammalian telomeres end in a large duplex loop. Cell. 1999; 97:503–14. [PubMed: 10338214]
4. de Lange T. T-loops and the origin of telomeres. Nat Rev Mol Cell Biol. 2004; 5:323–9. [PubMed: 15071557]
5. Doksani Y, Wu JY, de Lange T, Zhuang X. Super-resolution fluorescence imaging of telomeres reveals TRF2-dependent T-loop formation. Cell. 2013; 155:345–56. [PubMed: 24120135]
6. Olovnikov AM. A theory of marginotomy. The incomplete copying of template margin in enzymic synthesis of polynucleotides and biological significance of the phenomenon. J Theor Biol. 1973; 41:181–90. [PubMed: 4754905]
7. Watson JD. Origin of concatemeric T7 DNA. Nat New Biol. 1972; 239:197–201. [PubMed: 4507727]
8. Wu P, Takai H, de Lange T. Telomeric 3′ overhangs derive from resection by Exo1 and Apollo and fill-in by POT1b-associated CST. Cell. 2012; 150:39–52. [PubMed: 22748632]

9. Kim NW, et al. Specific association of human telomerase activity with immortal cells and cancer. Science. 1994; 266:2011–5. [PubMed: 7605428]
10. Wright WE, Piatyszek MA, Rainey WE, Byrd W, Shay JW. Telomerase activity in human germline and embryonic tissues and cells. Dev Genet. 1996; 18:173–9. [PubMed: 8934879]
11. Cohen SB, et al. Protein composition of catalytically active human telomerase from immortal cells. Science. 2007; 315:1850–3. [PubMed: 17395830]
12. Bryan TM, Englezou A, Dalla-Pozza L, Dunham MA, Reddel RR. Evidence for an alternative mechanism for maintaining telomere length in human tumors and tumor-derived cell lines. Nat Med. 1997; 3:1271–4. [PubMed: 9359704]
13. Londono-Vallejo JA, Der-Sarkissian H, Cazes L, Bacchetti S, Reddel RR. Alternative lengthening of telomeres is characterized by high rates of telomeric exchange. Cancer Res. 2004; 64:2324–7. [PubMed: 15059879]
14. Yeager TR, et al. Telomerase-negative immortalized human cells contain a novel type of promyelocytic leukemia (PML) body. Cancer Res. 1999; 59:4175–9. [PubMed: 10485449]
15. Bryan TM, Englezou A, Gupta J, Bacchetti S, Reddel RR. Telomere elongation in immortal human cells without detectable telomerase activity. EMBO J. 1995; 14:4240–8. [PubMed: 7556065]
16. Oganesian L, Karlseder J. Mammalian 5′ C-rich telomeric overhangs are a mark of recombination-dependent telomere maintenance. Mol Cell. 2011; 42:224–36. [PubMed: 21504833]
17. Tokutake Y, et al. Extra-chromosomal telomere repeat DNA in telomerase-negative immortalized cell lines. Biochem Biophys Res Commun. 1998; 247:765–72. [PubMed: 9647768]
18. Cesare AJ, Griffith JD. Telomeric DNA in ALT cells is characterized by free telomeric circles and heterogeneous t-loops. Mol Cell Biol. 2004; 24:9948–57. [PubMed: 15509797]
19. Henson JD, et al. DNA C-circles are specific and quantifiable markers of alternative-lengthening-of-telomeres activity. Nat Biotechnol. 2009; 27:1181–5. [PubMed: 19935656]
20. Sharpless NE, DePinho RA. How stem cells age and why this makes us grow old. Nat Rev Mol Cell Biol. 2007; 8:703–13. [PubMed: 17717515]
21. Aubert G. Telomere dynamics and aging. Prog Mol Biol Transl Sci. 2014; 125:89–111. [PubMed: 24993699]
22. Zeng S, et al. Telomerase-mediated telomere elongation from human blastocysts to embryonic stem cells. J Cell Sci. 2014; 127:752–62. [PubMed: 24338368]
23. Batista LF, et al. Telomere shortening and loss of self-renewal in dyskeratosis congenita induced pluripotent stem cells. Nature. 2011; 474:399–402. [PubMed: 21602826]
24. Raices M, et al. C. elegans telomeres contain G-strand and C-strand overhangs that are bound by distinct proteins. Cell. 2008; 132:745–57. [PubMed: 18329362]
25. Pickett HA, Cesare AJ, Johnston RL, Neumann AA, Reddel RR. Control of telomere length by a trimming mechanism that involves generation of t-circles. EMBO J. 2009; 28:799–809. [PubMed: 19214183]
26. Pickett HA, Henson JD, Au AY, Neumann AA, Reddel RR. Normal mammalian cells negatively regulate telomere length by telomere trimming. Hum Mol Genet. 2011; 20:4684–92. [PubMed: 21903669]
27. Nabetani A, Ishikawa F. Unusual telomeric DNAs in human telomerase-negative immortalized cells. Mol Cell Biol. 2009; 29:703–13. [PubMed: 19015236]
28. Wang RC, Smogorzewska A, de Lange T. Homologous recombination generates T-loop-sized deletions at human telomeres. Cell. 2004; 119:355–68. [PubMed: 15507207]
29. O'Sullivan RJ, et al. Rapid induction of alternative lengthening of telomeres by depletion of the histone chaperone ASF1. Nat Struct Mol Biol. 2014; 21:167–74. [PubMed: 24413054]
30. Marion RM, et al. Telomeres acquire embryonic stem cell characteristics in induced pluripotent stem cells. Cell Stem Cell. 2009; 4:141–54. [PubMed: 19200803]
31. Agarwal S, et al. Telomere elongation in induced pluripotent stem cells from dyskeratosis congenita patients. Nature. 2010; 464:292–6. [PubMed: 20164838]
32. Wang F, et al. Molecular insights into the heterogeneity of telomere reprogramming in induced pluripotent stem cells. Cell Res. 2012; 22:757–68. [PubMed: 22184006]

33. Panopoulos AD, et al. Rapid and highly efficient generation of induced pluripotent stem cells from human umbilical vein endothelial cells. PLoS One. 2011; 6:e19743. [PubMed: 21603572]
34. Panopoulos AD, et al. The metabolome of induced pluripotent stem cells reveals metabolic changes occurring in somatic cell reprogramming. Cell Res. 2012; 22:168–77. [PubMed: 22064701]
35. Poole LA, et al. SMARCAL1 maintains telomere integrity during DNA replication. Proc Natl Acad Sci U S A. 2015; 112:14864–9. [PubMed: 26578802]
36. Rizzo A, et al. Stabilization of quadruplex DNA perturbs telomere replication leading to the activation of an ATR-dependent ATM signaling pathway. Nucleic Acids Res. 2009; 37:5353–64. [PubMed: 19596811]
37. Lin W, et al. Mammalian DNA2 helicase/nuclease cleaves G-quadruplex DNA and is required for telomere integrity. EMBO J. 2013; 32:1425–39. [PubMed: 23604072]
38. Thangavel S, et al. DNA2 drives processing and restart of reversed replication forks in human cells. J Cell Biol. 2015; 208:545–62. [PubMed: 25733713]
39. Sfeir A, et al. Mammalian telomeres resemble fragile sites and require TRF1 for efficient replication. Cell. 2009; 138:90–103. [PubMed: 19596237]
40. Oganesian L, Karlseder J. 5′ C-rich telomeric overhangs are an outcome of rapid telomere truncation events. DNA Repair (Amst). 2013; 12:238–45. [PubMed: 23347616]
41. Compton SA, Choi JH, Cesare AJ, Ozgur S, Griffith JD. Xrcc3 and Nbs1 are required for the production of extrachromosomal telomeric circles in human alternative lengthening of telomere cells. Cancer Res. 2007; 67:1513–9. [PubMed: 17308089]
42. Cesare AJ, Reddel RR. Alternative lengthening of telomeres: models, mechanisms and implications. Nat Rev Genet. 2010; 11:319–30. [PubMed: 20351727]
43. Niida H, et al. Telomere maintenance in telomerase-deficient mouse embryonic stem cells: characterization of an amplified telomeric DNA. Mol Cell Biol. 2000; 20:4115–27. [PubMed: 10805753]
44. Wang Y, et al. An increase in telomere sister chromatid exchange in murine embryonic stem cells possessing critically shortened telomeres. Proc Natl Acad Sci U S A. 2005; 102:10256–60. [PubMed: 16000404]
45. Zalzman M, et al. Zscan4 regulates telomere elongation and genomic stability in ES cells. Nature. 2010; 464:858–63. [PubMed: 20336070]
46. Sexton AN, et al. Genetic and molecular identification of three human TPP1 functions in telomerase action: recruitment, activation, and homeostasis set point regulation. Genes Dev. 2014; 28:1885–99. [PubMed: 25128433]
47. Winkler T, et al. Defective telomere elongation and hematopoiesis from telomerase-mutant aplastic anemia iPSCs. J Clin Invest. 2013; 123:1952–63. [PubMed: 23585473]
48. Moon DH, et al. Poly(A)-specific ribonuclease (PARN) mediates 3′-end maturation of the telomerase RNA component. Nat Genet. 2015; 47:1482–8. [PubMed: 26482878]
49. Gu BW, et al. Impaired Telomere Maintenance and Decreased Canonical WNT Signaling but Normal Ribosome Biogenesis in Induced Pluripotent Stem Cells from X-Linked Dyskeratosis Congenita Patients. PLoS One. 2015; 10:e0127414. [PubMed: 25992652]
50. Verdun RE, Karlseder J. The DNA damage machinery and homologous recombination pathway act consecutively to protect human telomeres. Cell. 2006; 127:709–20. [PubMed: 17110331]
51. Zhong ZH, et al. Disruption of telomere maintenance by depletion of the MRE11/RAD50/NBS1 complex in cells that use alternative lengthening of telomeres. J Biol Chem. 2007; 282:29314–22. [PubMed: 17693401]
52. Takata M, et al. Chromosome instability and defective recombinational repair in knockout mutants of the five Rad51 paralogs. Mol Cell Biol. 2001; 21:2858–66. [PubMed: 11283264]
53. Dumon-Jones V, et al. Nbn heterozygosity renders mice susceptible to tumor formation and ionizing radiation-induced tumorigenesis. Cancer Res. 2003; 63:7263–9. [PubMed: 14612522]
54. Gilson E, Geli V. How telomeres are replicated. Nat Rev Mol Cell Biol. 2007; 8:825–38. [PubMed: 17885666]

55. Martinez P, et al. Increased telomere fragility and fusions resulting from TRF1 deficiency lead to degenerative pathologies and increased cancer in mice. Genes Dev. 2009; 23:2060–75. [PubMed: 19679647]
56. Betous R, et al. SMARCAL1 catalyzes fork regression and Holliday junction migration to maintain genome stability during DNA replication. Genes Dev. 2012; 26:151–62. [PubMed: 22279047]
57. Ahuja AK, et al. A short G1 phase imposes constitutive replication stress and fork remodelling in mouse embryonic stem cells. Nat Commun. 2016; 7:10660. [PubMed: 26876348]
58. Gohring J, Fulcher N, Jacak J, Riha K. TeloTool: a new tool for telomere length measurement from terminal restriction fragment analysis with improved probe intensity correction. Nucleic Acids Res. 2014; 42:e21. [PubMed: 24366880]
59. Ludwig TE, et al. Derivation of human embryonic stem cells in defined conditions. Nat Biotechnol. 2006; 24:185–7. [PubMed: 16388305]
60. Wong JM, Collins K. Telomerase RNA level limits telomere maintenance in X-linked dyskeratosis congenita. Genes Dev. 2006; 20:2848–58. [PubMed: 17015423]
61. O'Sullivan RJ, Kubicek S, Schreiber SL, Karlseder J. Reduced histone biosynthesis and chromatin changes arising from a damage signal at telomeres. Nat Struct Mol Biol. 2010; 17:1218–25. [PubMed: 20890289]
62. Sarbassov DD, Guertin DA, Ali SM, Sabatini DM. Phosphorylation and regulation of Akt/PKB by the rictor-mTOR complex. Science. 2005; 307:1098–101. [PubMed: 15718470]
63. Ruiz S, et al. A high proliferation rate is required for cell reprogramming and maintenance of human embryonic stem cell identity. Curr Biol. 2011; 21:45–52. [PubMed: 21167714]
64. Cesare AJ, et al. Spontaneous occurrence of telomeric DNA damage response in the absence of chromosome fusions. Nat Struct Mol Biol. 2009; 16:1244–51. [PubMed: 19935685]
65. Karlseder J, Smogorzewska A, de Lange T. Senescence induced by altered telomere state, not telomere loss. Science. 2002; 295:2446–9. [PubMed: 11923537]
66. Zellinger B, Akimcheva S, Puizina J, Schirato M, Riha K. Ku suppresses formation of telomeric circles and alternative telomere lengthening in Arabidopsis. Mol Cell. 2007; 27:163–9. [PubMed: 17612498]

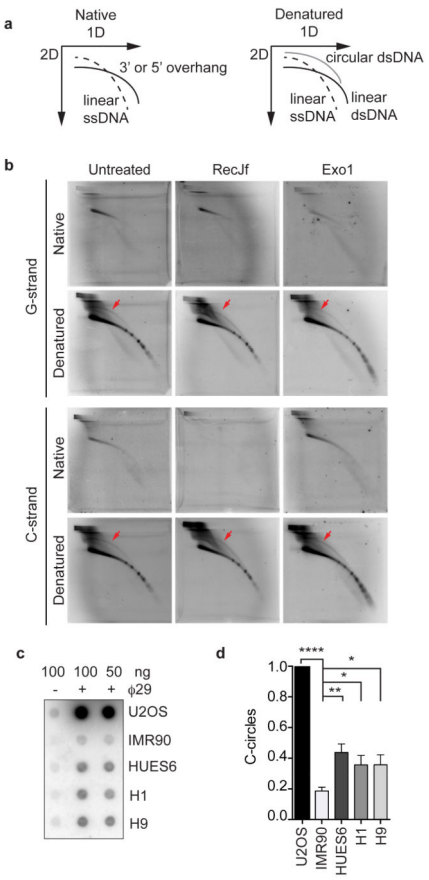

Figure 1. hESCs contain cytosine-rich telomeric overhang and extrachromosomal telomeric repeats

(a) Schematic representation of 2D gel electrophoresis, which allows the separation of DNA according to the molecular weight (1D) and conformation (2D). DNA overhangs and extrachromosomal ss DNA are visualized under native conditions. Linear or circular ds telomeric DNA are detected on denatured gels.

(b) Native and denatured 2D gels of genomic DNA from HUES6 cells, probed for DNA of G-rich (top panels) or C-rich (bottom panels) telomeric sequence. 5′-3′ (RecJf) or 3′-5′ (Exo1) exonuclease treatment prior to separation is indicated. Red arrows point at the arcs resulting from circular dsDNA (T-circles).

(c) C-circle assay in U20S, IMR90, HUES6, H1 and H9 cells. 100 and 50 ng of restriction-digested genomic DNA were used in each assay. The dot blot was hybridized with ^{32}P end-labelled $(CCCTAA)_5$ oligonucleotide probe.

(d) Quantification of C-circles in U2OS, IMR90, HUES6, H1 and H9 cells. Levels are calculated relative to those of U20S cells. Data represent means ± s.e.m of four experiments. **** P <0.0001, ** P <0.01, * P <0.05 (two-tailed Student's t-test).

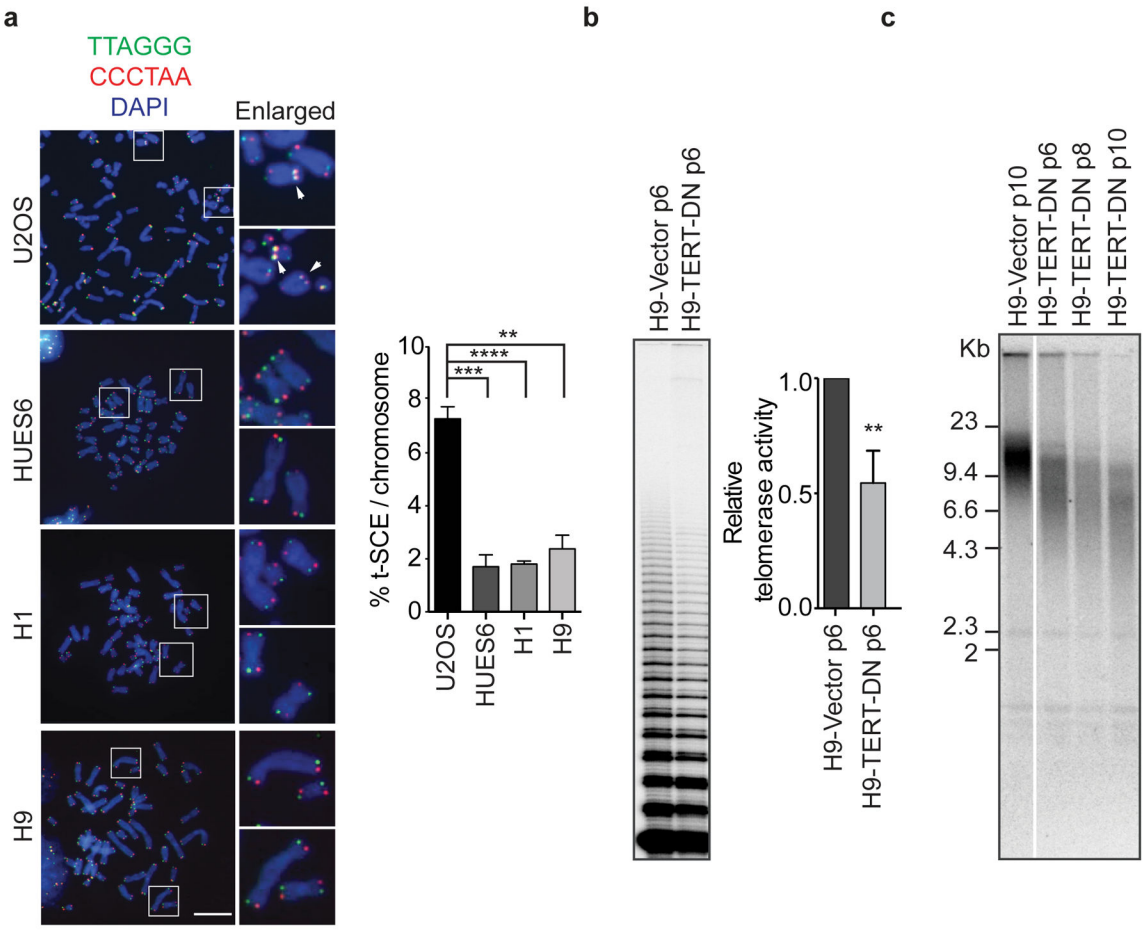

Figure 2. Telomerase-dependent telomere elongation in hESCs

(a) Representative images of CO-FISH metaphases from U2OS, HUES6, H1 and H9 cells. White arrows indicate t-SCEs. Green, $(CCCTAA)_n$ probe; Red, $(TTAGGG)_n$ probe. DNA was stained with DAPI (blue). Scale bar, 10 μm. Quantification of t-SCEs from CO-FISH analysis of the indicated cells is shown on the right. Data represent means ± s.e.m of three experiments (≥30 metaphases/experiment). ****$P < 0.0001$, ***$P < 0.001$, **$P < 0.01$ (two-tailed Student's *t*-test).

(b) TRAP assay of vector control and dominant negative (DN) TERT transduced H9 cells. Quantification is shown on the right. Data represent relative telomerase activity compared to control cells, n=3, (mean ± s.d.). **$P < 0.01$ (two-tailed Student's *t*-test).

(c) Telomere restriction fragment length assay of H9 cells following control or TERT-DN transduction. Uncropped blot image is shown in Supplementary Data Set 1.

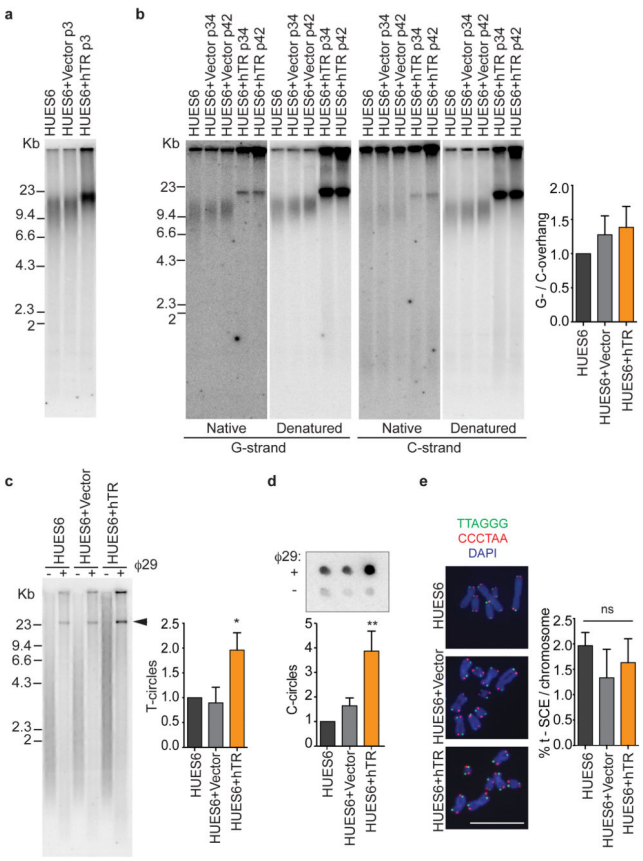

Figure 3. Telomere elongation stimulates the formation of extrachromosomal telomeric repeats in hESCs

(a) Telomere restriction fragment length assay of HUES6 cells and HUES6 cells stably expressing vector control or hTR on passage 3 after selection.

(b) 1D gels of restriction digested genomic DNA from parental HUES6 and HUES6 cells 34 and 42 passages post control or hTR transduction. The gels were probed for G- and C-rich telomeric DNA under native and denatured conditions. The overhang signal in native gels was normalized against the total amount of telomeric DNA in denatured gels. Data represent means ± s.d of three independent experiments.

(c) T-circle assay of 1 μg of digested genomic DNA from HUES6, vector control or hTR cells. The presence or absence of ϕ29 DNA polymerase is indicated. Quantification of T-circle products (arrow) is calculated relative to untreated cells and normalized against the signal from the reaction lacking ϕ29 polymerase. Data represent means ± s.e.m of three independent experiments. *P <0.05 (two-tailed Student's t-test).

(d) C-circle assay for 100 ng of digested genomic DNA from HUES6, vector control or hTR cells. Quantification of C-circle levels (bottom) from three independent experiments. Data represent means ± s.d. **P <0.01 (two-tailed Student's t-test).

(e) Representative images of CO-FISH metaphases from HUES6, control or hTR cells. Scale bar, 10 μm. The quantification of t-SCE events showing means ± s.e.m from three independent experiments is shown on the right. Ns, not significant (two-tailed Student's t-test).

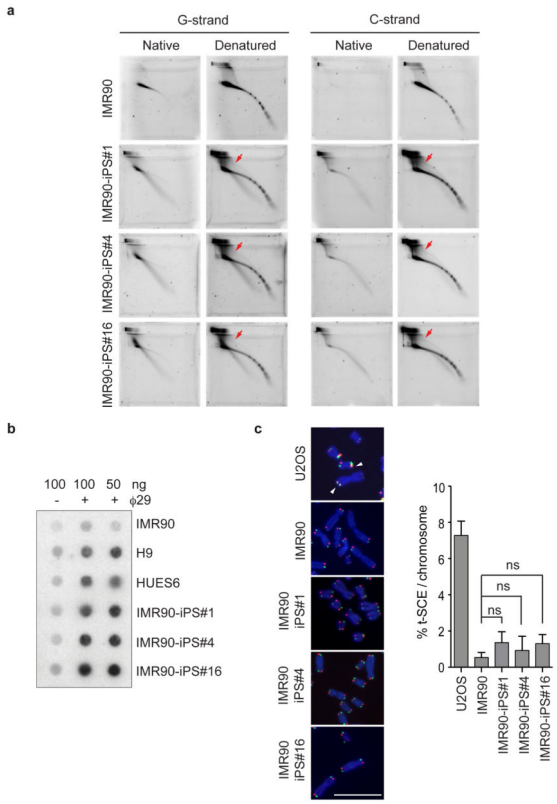

Figure 4. Reprogramming of human differentiated cells induces the accumulation of cytosine-rich telomeric overhang and extrachromosomal telomeric repeats

(a) Restriction-digested genomic DNA from human IMR90, and IMR90-iPS cell lines was electrophoresed in two dimensions and probed for DNA of G-rich (left panels) or C-rich (right panels) telomeric sequence under native and denatured conditions. Red arrows indicate T-circles.

(b) C-circle assay in IMR90, H9, HUES6 and IMR90-iPS cell lines. The dot blot was hybridized with ^{32}P end-labeled $(CCCTAA)_5$ oligonucleotide probe.

(c) Representative images of CO-FISH metaphases from IMR90 and IMR90-iPS cells. U2OS cells were included as a positive control. White arrowheads indicate t-SCEs. Scale bar, 10 μm. Quantification of t-SCE from CO-FISH analysis is shown on the right. Data represent means ± s.d of three independent experiments (≥25 metaphases/experiment). Ns, not significant (two-tailed Student's *t*-test).

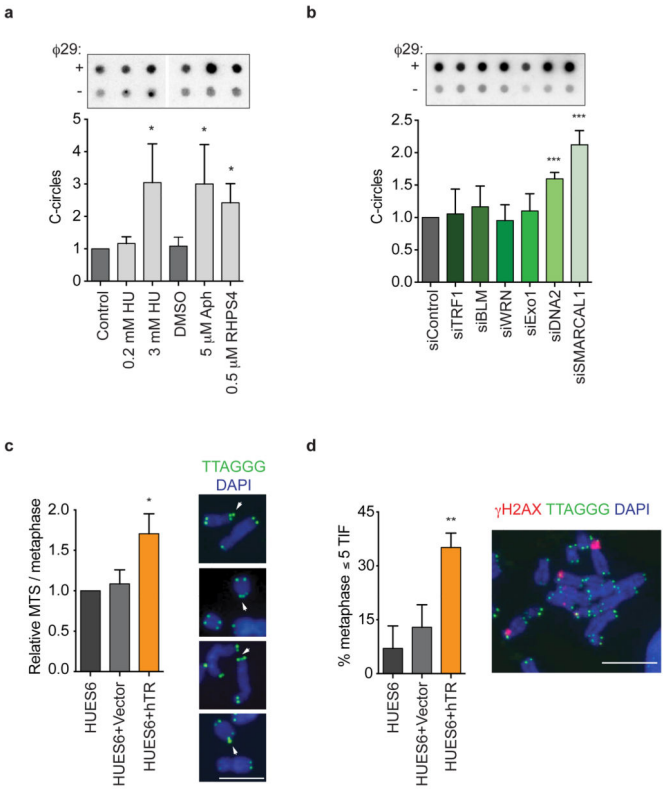

Figure 5. DNA replication stress causes the accumulation of C-circles in hESCs

(a) HUES6+hTR cells were treated with 0.2 mM, 3 mM HU, 5 μM Aphidicolin (Aph) or 0.5 μM RHPS4 for 24 h before analyzed for C-circle formation. 100 ng of digested genomic DNA was used in each condition. The quantification (bottom) is from five independent experiments. C-circle levels are calculated relative to the levels in control treated cells. Data represent means ± s.e.m. *P <0.05 (two-tailed Mann-Whitney test). Uncropped blot image is shown in Supplementary Data Set 1.

(b) C-circle assay for 100 ng of digested genomic DNA from untreated HUES6+hTR or transfected with the indicated siRNAs. The quantification (bottom) is calculated relative to the levels in siControl treated cells. Data represent means ± s.e.m of three independent experiments. ***P <0.001 (two-tailed Student's t-test).

(c) Quantification of metaphase chromosomes with MTS in hESCs with overextended telomeres relative to control cells. Data represent means ± s.e.m of six independent experiments (≥30 metaphases/experiment). *P <0.05 (two-tailed Student's t-test). Representative images of chromosomes with MTS (white arrowheads) are shown on the right. DAPI (blue), telomere FISH (green). Scale bar, 5 μm.

(d) Quantification of γ-H2AX associated telomeres in meta-TIF assays in parental, vector control or hTR overexpressing HUES6 cells. The mean and s.d of three independent experiments are shown (≥25 metaphases/experiment). **P <0.01 (two-tailed Student's t-test). Representative image from meta-TIF assay is shown on the right. DAPI (blue), telomere FISH (green) and γ-H2AX (red) IF. Scale bar, 10 μm.

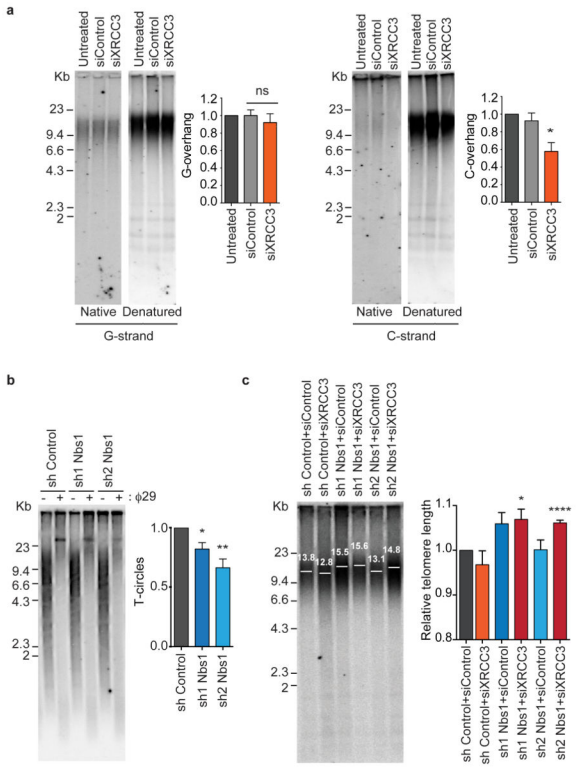

Figure 6. XRCC3 and Nbs1 contribute to the formation of 5′ C-rich telomeric DNA and T-circles and regulate telomere length in hESCs

(a) HUES6 cells were transfected with siControl or siXRCC3 and analyzed for G-rich and C-rich telomeric DNA in 1D gels under native and denatured conditions. Quantification of the overhangs signal is shown on the right. The amount of G-rich and C-rich ss telomeric DNA in native gels was normalized against the total amount of telomeric DNA in denatured gels. Values are calculated relative to untreated cells from five independent experiments (means ± s.e.m). *P <0.05; ns, not significant (two-tailed Student's t-test).

(b) T-circle assay from HUES6 cells infected with shScramble or shRNAs against Nbs1. Samples were analyzed 5 days post-transduction. Relative T-circle levels normalized against the signal without ϕ29 DNA polymerase from three independent experiments are shown on the right (means ± s.e.m). *P <0.05, **P <0.01 (two-tailed Student's t-test).

(c) Telomere length was analyzed by TRF analysis 7 days following the indicated knockdowns of XRCC3 and Nbs1. Mean telomere length is shown in each condition calculated with TeloTool software[58]. Quantification of telomere length fold change relative to control samples is shown on the right. Data represent means ± s.e.m between four independent experiments. ****P < 0.0001, *P <0.05 (two-tailed Student's t-test).

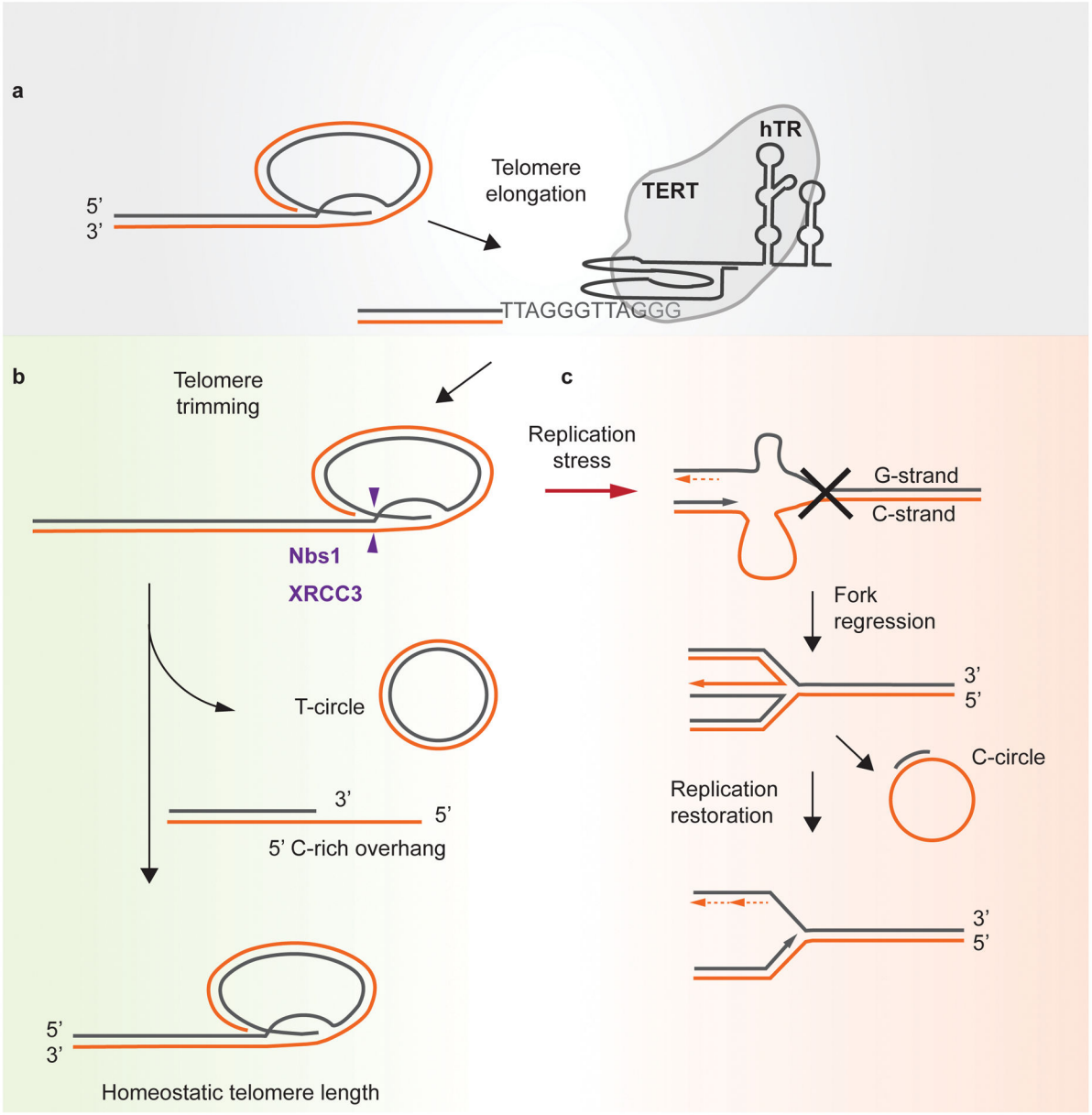

Figure 7.

Proposed model for telomere length regulation in hESCs. (a) Telomere elongation occurs through the telomerase dependent pathway, and is counteracted by trimming mechanisms mediated by XRCC3 and Nbs1 (b). The activity of XRCC3 and Nbs1 is required to promote the resolution of T-loops giving rise to ss 5′ C-rich telomeric DNA and T-circles. Both HR factors are essential to compensate for excessive telomere elongation. (c) Long telomeres are prone to replicative stress resulting in the formation of C-circles. We speculate that C-circles are generated by resolution of replication intermediates after replication fork stalling.